

## Regular Paper

---

# On the response of fluidized piles from laboratory model tests in granular soils

F. Schnaid\*, L. Passini, F. Stracke and S. Mezzomo

*Federal University of Rio Grande do Sul, Brazil*

**Abstract.** Design guidelines of foundation anchors and piles embedded in fluidized sand comprises understanding of installation processes, defining constitutive parameters and establishing analysis techniques. These fundamental aspects have been investigated by a series of laboratory model tests designed to evaluate the mechanism taking place during pile installation through the influence of downwardly-directed vertical water jets in the geometry of fluidized cavities in saturated sands. Measurements indicate fluidization geometry to be controlled by combined effects of jet velocity and the ratio of particle and jet diameters which can be conveniently expressed by the Froude number of particles. Characteristics of the fluidized zone geometry prior and after fluidization indicate considerable reduction of relative density of fluidized samples. Limit equilibrium analysis using geotechnical parameters approaching critical state provided indicative horizontal stress levels to estimate the uplift skin friction of model steel piles.

Keywords: Fluidization, sands, piles

## 1. Introduction

Fluidization is defined as the suspension of particles due to the action of an upward fluid flow. General principles and mechanisms of fluidization in granular soils have been comprehensively analysed and have given rise to a number of applications in the field of channelling [23, 32, 33], erosion [1], removal of sediments and remediation of contaminants (e.g. [3, 6, 22, 24]). Despite being a common feature in several disciplines, the application of fluidization processes to foundation engineering is not well understood and possible applications have not been fully explored. Although empirical approaches provide valuable insights for onshore, nearshore and offshore foundations (e.g. [4, 9, 11]), there is no standardized design methodology. Under current configurations, there is scope to provide recommendations to optimise the jetting performance by verifying some of the essential features of the fluidization process that occurs as a jet is lowered into a granular medium. Implications of the fluidization process to piles analysis and design are discussed on the light of critical state soil mechanics.

## 2. Materials and methods

Fluidization, piezocone and load tests were carried out in rectangular acrylic chambers with internal dimensions of 478 mm × 278 mm × 320 mm and 450 mm × 450 mm × 1100 mm high (Fig. 1a, c). Siliceous sand specimen prepared using the moist tamping method were carefully inundated by water percolating upwards until it reaches a water constant head of 5 cm above the soil surface. It is then maintained constant throughout the test to ensure that the flow rate and therefore the jet velocity are constant.

---

\*Corresponding author: F. Schnaid, Federal University of Rio Grande do Sul, Brazil. E-mails: fernando@ufrgs.br; fschnaid@gmail.com.

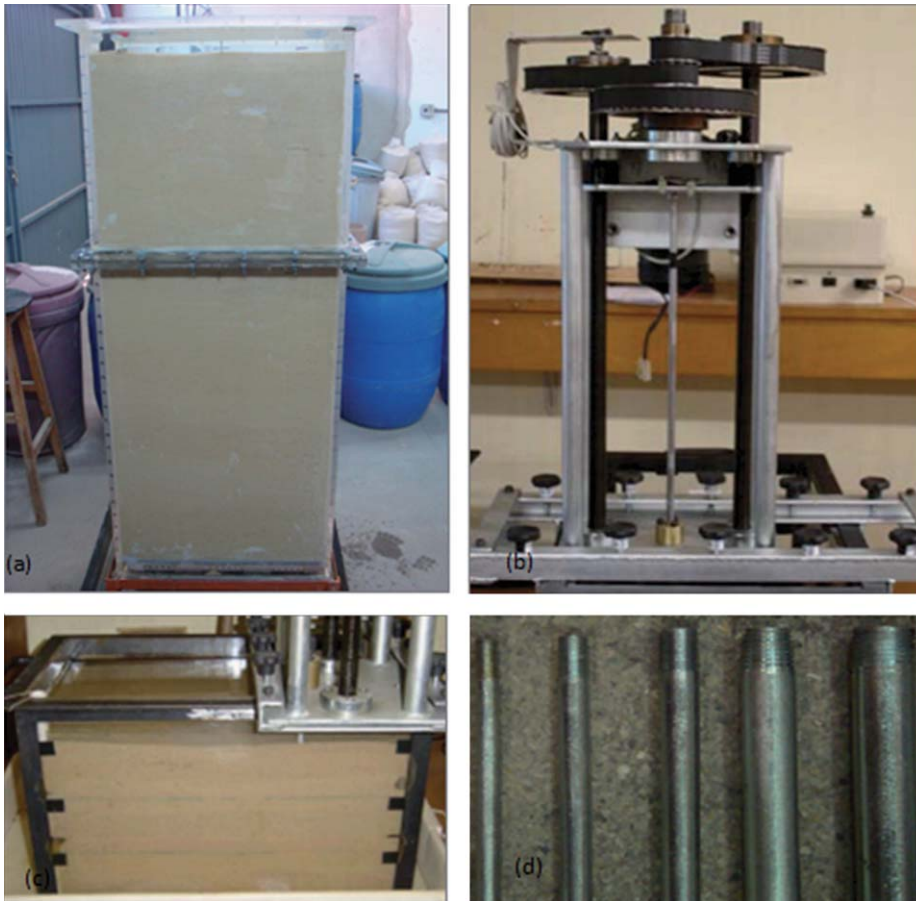


Fig. 1. Details of (a, c) fluidization chambers, (b) supporting frame and (d) metal tubes.

To start the test, a metal tube is positioned vertically on the soil surface, being lowered in increments during the jetting stage. Carbon steel metal tubes have been used with internal diameters ranging from 3.85 mm to 12 mm (Fig. 1d). A downwardly-directed vertical water jet velocity is applied through the tubes and at the end of each stage, after completion of the fluidization process, the tube is repositioned in increasing depths within the chamber. A supporting structure equipped with a ball-screw allowed the gradual displacement of the tubes at any location below the sand surface in a precise upright position (Fig. 1b). The descent of the tubes is conducted in 20 mm increments along the depth.

A schematic representation of the experimental setup is presented in Fig. 2. The hydraulic circuit consists on a PVC pipeline where the water from a 500 liter's reservoir flows driven by a centrifugal pump. The pump motor is connected to a frequency inverter, which regulates the rotation speed of the pump and thus the flow rate, measured by a rotameter. The insertion tubes are the final part of the circuit. The water produces a jet emanating from the tubes that fluidizes the soil zone when inserted inside the sand.

The tubes installed into the soil were later used as prototype piles to perform load tests using the steel casing attached to the chamber as a reaction frame. A seating load varying from 1 to 7 N (corresponding to the actual weight of the pile) was applied prior to zeroing the dial gauges and additional load was then applied in small increments ranging from 10 to 15 percent of the design load and maintained for a few minutes (necessary for complete stabilization of displacements).

Two sands have been tested, corresponding to the fine and coarse particle size distribution shown in Fig. 3. The fine sand comes from a natural deposit located in Brazil (Osorio Sand), while the coarse sand is a material selected

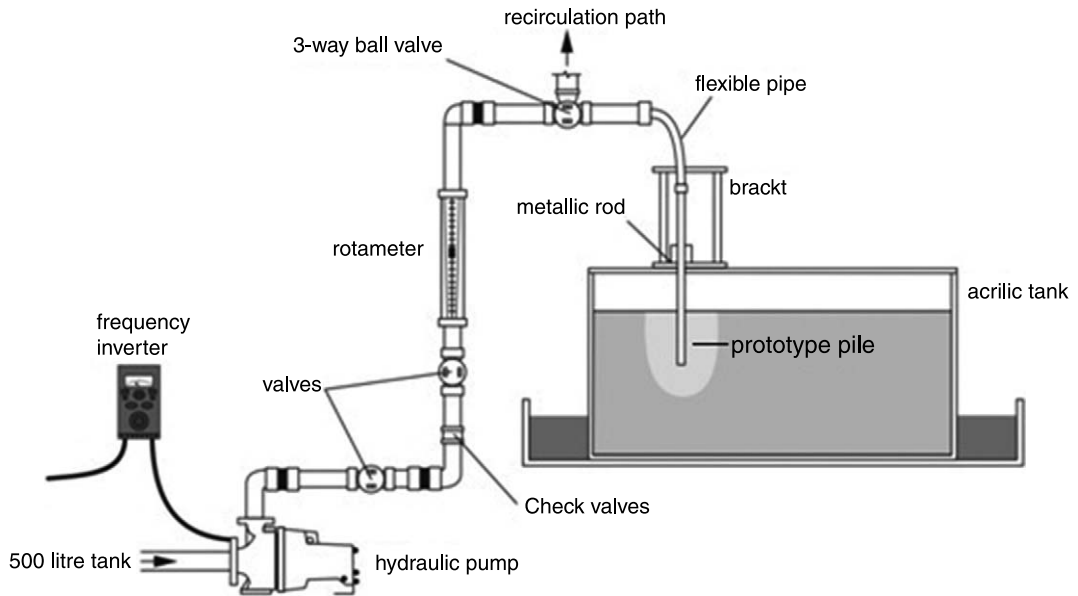


Fig. 2. Schematic representation of the experimental setup.

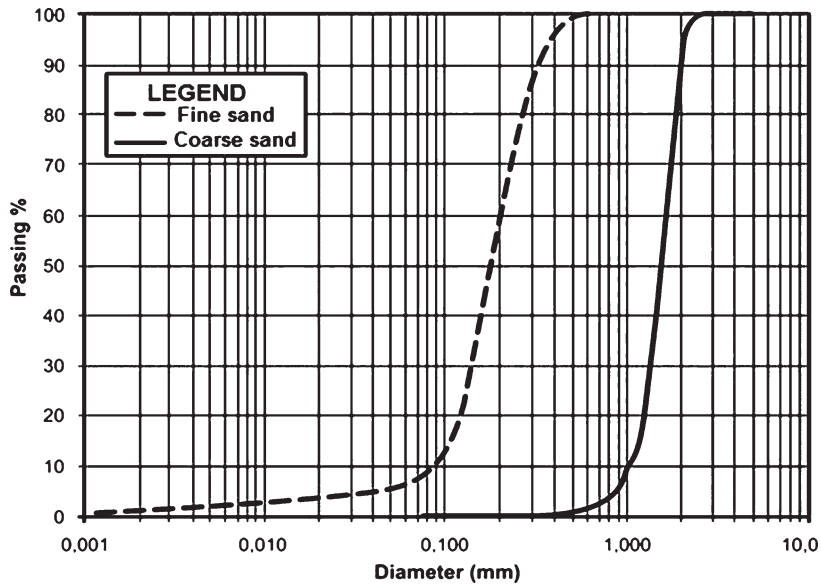


Fig. 3. Particle size distribution.

by sieving. Characterization of these two uniform, quartz, clean sands is presented in Table 1. Sand specimens are obtained by deposition inside the acrylic box at relative densities of 50% and 90%.

### 3. Installation mechanism

The installation mechanism was evaluated from experiments conceived to demonstrate that turbulent shear produced by downwardly-directed vertical water jet spreads radially, forming a fluidized zone surrounded by a circular

Table 1  
Soil properties

Characteristics	Fine sand	Coarse sand
Specific Gravity of Solid Particles ( $G_s$ )	2667 kg/m <sup>3</sup>	2673 kg/m <sup>3</sup>
Effective diameter ( $D_{10}$ )	0.09 mm	1.04 mm
Mean diameter ( $D_{50} = d_p$ )	0.18 mm	1.56 mm
Minimum void ratio ( $e_{\min}$ )	0.60	0.61
Maximum void ratio ( $e_{\max}$ )	0.90	0.88
Coefficient of hydraulic conductivity (k)	$1.3 \times 10^{-4}$ m/s	$1.1 \times 10^{-2}$ m/s

Table 2  
Sand and flow parameters

N° tests	Sand	$d_j$ (mm)	$Q_o$ (L/min)	$U_o$ (m/s)	$Fr_p$
43	Fine	3.85–12.0	0.70–6.4	0.13–4.15	2.37–77.46
20	Coarse	3.85–12.0	0.70–6.8	0.64–4.29	2.76–26.84

dune of eroded, redeposited material (e.g. [22, 24, 34]). With increasing jet depth this fluidized zone undergo a transition from an open, approximately ellipsoidal form to an asymmetric spouted zone and finally to a submerged cavity [21, 22]. The basic geometry conceived to describe a cavity formed by the jetting mechanism is illustrated in Fig. 4 and is expressed by a group of geometry parameters comprising jet velocity  $U_o$ , gravitational constant  $g$ , particle diameter  $d_p$ , fluid density  $\rho_f$ , solids density  $\rho_s$ . Steady state depths and radii of fluidization zones are shown to be generally proportional to the dimensionless Froude number  $Fr$ , defined as the ratio of a characteristic velocity to a gravitational wave velocity, being conveniently defined as the Froude number of particles:

$$Fr_p = \frac{U_o}{\sqrt{d_p \left( \frac{\rho_s - \rho_f}{\rho_f} \right) g}} \quad (1)$$

For tests carried out in the present study, for each depth, the tube was held in a fixed position and measurements of the fluidized zone geometry were recorded. After completion of each stage, the tube was lowered and the procedure repeated. Experiments were conducted with the jet positioned in the centre of the tank and adjacent to the tank wall for observation purposes. In this last case, the geometric information was obtained by direct observation through the walls of the acrylic tank covered with a plastic film to allow tracing of fluidized contours of the cavity. In addition experiments have been photographed and filmed.

For any given sand, three groups of tests have been carried out as outlined below.

- Constant flow rate ( $Q_o$ ) with variations in the injection diameter ( $d_j$ ) and jet velocity ( $U_o$ )
- Constant jet velocity ( $U_o$ ) with variations in the injection diameter ( $d_j$ ) and flow rate ( $Q_o$ )
- Constant injection diameter ( $d_j$ ) with variations in jet velocity ( $U_o$ ) and flow rate ( $Q_o$ )

Controlled variables are the injection diameter ( $d_j$ ), that is the same of the internal pile diameter ( $d_i$ ), external pile diameter ( $d_e$ ), pile length inside sand specimen ( $L$ ), sand physical properties, water height above the soil ( $h_w$ ) and the dimensions of the tank. Measured parameters are the flow rate ( $Q_o$ ), temperature of the water and the geometry of the steady state fluidized zone which is all represented in Fig. 4. A series of 63 tests in lateral position inside the tank was carried out to evaluate the influence of flow rate in the range of 0.70 and 6.80 L/min and jet velocity in the range 0.13 to 4.29 m/s, as summarized in Table 2. Since the viscosity of the water is affected by temperature, the water temperature was kept constant at  $20 \pm 1^\circ\text{C}$  throughout experiments.

The geometry of the fluidized zone after completion of the test procedure is presented in Fig. 5a. During fluidization a steady state profile is formed exhibiting a concave upward sharp interface between fluidized and surrounding non-fluidized soil. The interface contour is drawn as a continuous line, with a vertical dashed line representing the axis of penetration of the jet and the dotted line the original sand surface. In this set of experiments a fully axisymmetric



radial flow percolates through the sand and may occasionally reach the boundaries, flowing upwards and out the tank, without affecting the actual geometry of the fluidized sand.

Direct observation of the measured steady state geometries indicates that, for a given sand and constant input parameters, the increase in flow rate leads to increasing  $d_H$  and  $a$  values. For a given flow, the diameter of the fluidized zone reduces with increasing average particle diameter ( $D_{50}$  or  $d_p$ ). As for the jet velocity, for a given sand and flow rate, the larger the diameter of the jet ( $d_j$ ) the lower the radii of the fluidized zone at the jet tip  $d_H$  and the jet penetration depth  $a$ . Consequently, as the jet velocity increases the diameter of the fluidized zone and the jet penetration depth also increase. The soil movement due to turbulent flow under high jet velocities extended up to 20 pile diameters from the side of the prototype piles and up to 30 diameters below the pile tip. The geometry of the fluidized zone reported here is representative of tubes fixed vertically and lowered into the ground in increments during the jet stage: this condition differs from piles lowered into the ground by the own self-weight during fluidization (to be addressed in a separate publication).

#### 4. Fluidized geometry

Results are interpreted on the bases of the geometrical parameters defined in Fig. 4, emphasizing the two parameters that control pile design: jet penetration depth  $a$  and diameter of fluidized zone at the pile tip  $d_H$ . Tests on fine sand are grouped in Fig. 6 and are used to illustrate the experimental testing conditions for different combinations of pile diameters, jet velocity and relative density. As seen in this figure both  $a$  and  $d_H$  remained approximately constant throughout the test, demonstrating that scour geometries can be conveniently scaled by the pile diameter  $d_j$ . Tests on coarse sand exhibit the same behavioural patten described for fine sand, with a slightly reduction in  $a/d_j$  and  $d_H/d_j$  as the jet depth approaches that of a cavity formation, at the critical depth.

Tests carried out in a given sand (fine, medium or course) and at a given jet velocity ( $U_o$ ) can be expressed by the Froude number of particles ( $Fr_p$ ), according to Equation 1. The variation of  $a/d_j$  versus  $Fr_p$  is plotted in Fig. 7, showing average data points corresponding to stable open profiles for a variety of fine and coarse sands, including data reported by Niven, 1998. In all sands the fluidization jet penetration depth  $a/d_j$  increases with increasing  $Fr_p$ . By multiple regression analysis, the value of  $a/d_j$  can be correlated to  $Fr_p$  by polynomial function:

$$\left(\frac{a}{d_j}\right) = 0.58Fr_p \quad r^2 = 0,93; \quad n = 131 \quad (2)$$

A similar analysis has been performed to estimate the fluidization radii at the jet tip  $d_H/d_j$ . Only open cavities are considered and average values are provided. As before, the variation of  $d_H/d_j$  and  $Fr_p$  is approached by polynomial equation, as represented in Fig. 8:

$$\left(\frac{d_H}{d_j}\right) = 0.57Fr_p \quad r^2 = 0,93; \quad n = 131 \quad (3)$$

There has been no influence of relative density in the geometry of the fluidized zone when the two governing parameters: jet penetration depth  $a$  and radii at the pile tip  $d_H$  are plotted in the  $Fr_p$  space.

In general terms, experiments have confirmed previous research, indicating the transition from an open to a submerged fluidized cavity. This transition occurs at a critical depth  $T$  that appears to be a complex function of the ability of the flow to support the weight of the overlaying fluidized bed, the turbulent nature of the scour process and the permeability of the surrounding soil [13, 22].

In the present study the critical depth has been clearly observed in experiments on coarse [20] and fine sands [30]. Measured critical depths comply with previously values reported by Niven [21]. The critical depth is shown to be a function of the flow rate  $Q_o$ , injection diameter  $d_j$  and jet velocity  $U_o$ , particle diameter  $d_p$  and coefficient of hydraulic conductivity  $k$  (to be addressed in a separate publication).

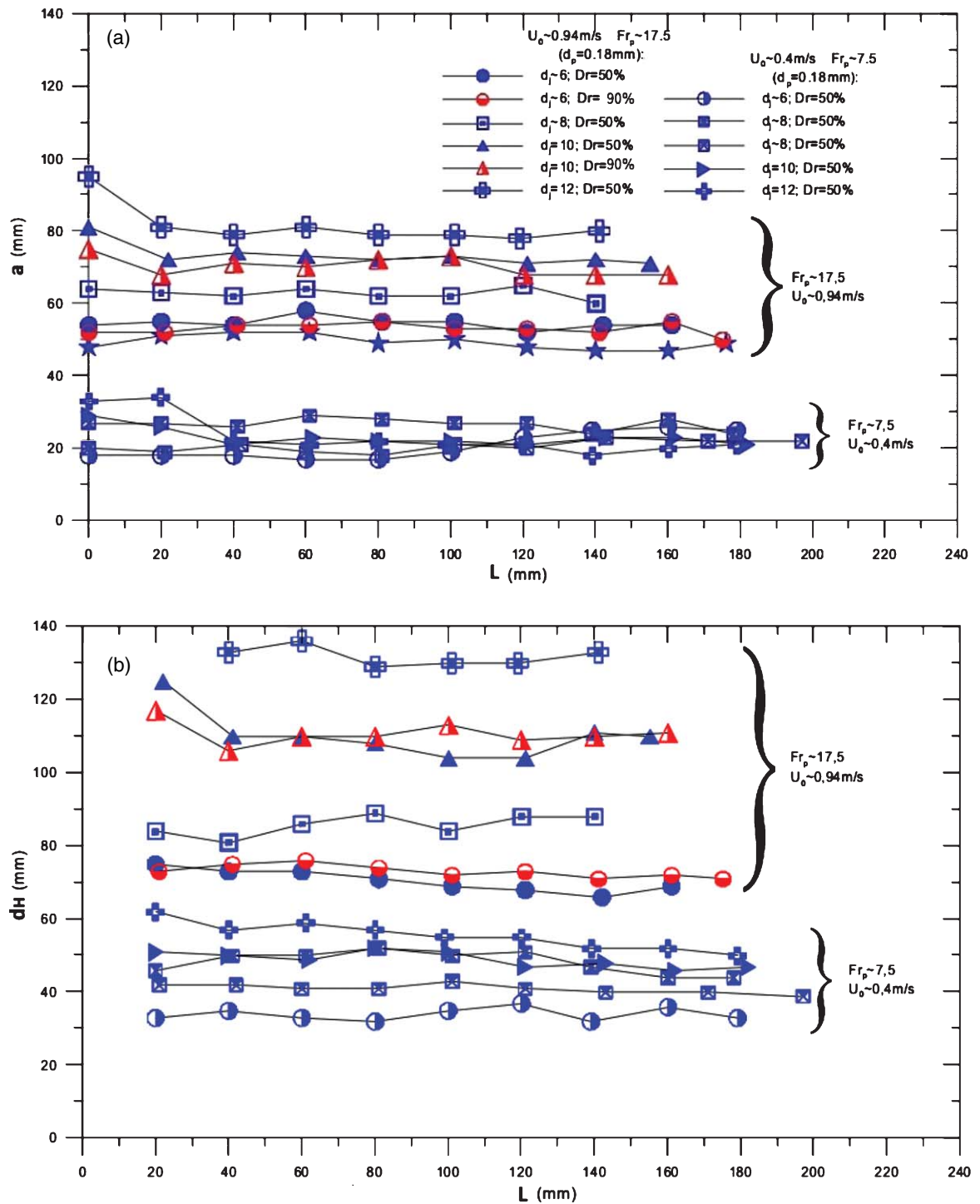


Fig. 6. (a) Jet penetration depth and (b) jet radii at the pile at tip plotted against pile length inside fine sand specimen.

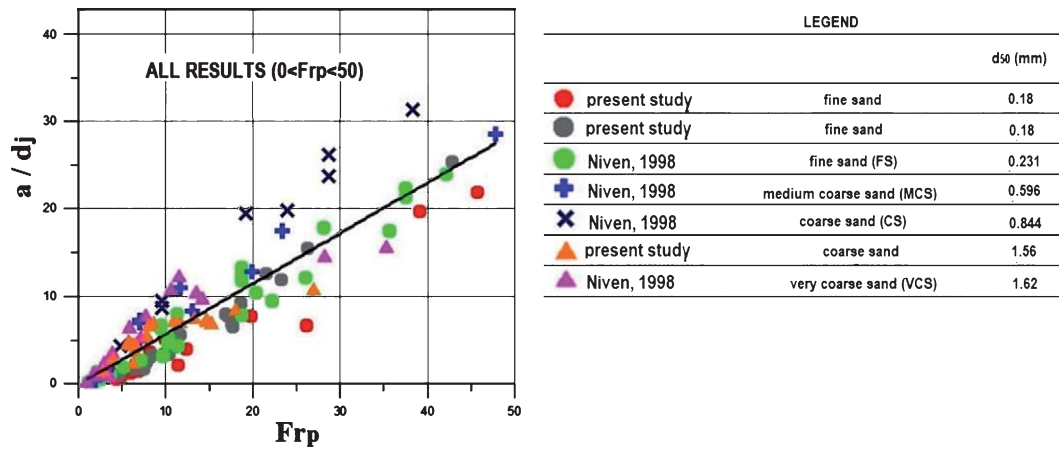


Fig. 7. Relation between fluidization jet penetration depth and Froude number for open submerged cavities.

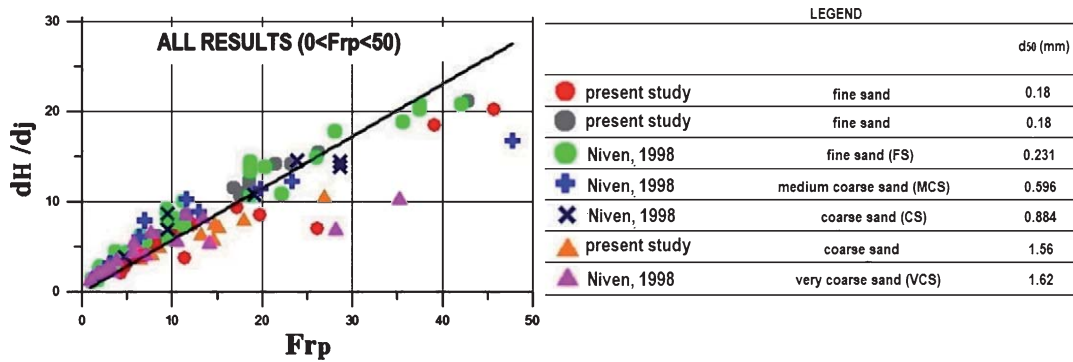


Fig. 8. Relation between fluidization radii at the jet tip and Froude number for open submerged cavities.

## 5. Sand density

Once the prediction of steady state fluidized zone geometry from system variables is completed, the additional requirement for foundation design is the density of the fluidized area after completion of fluidized cycle. During fluidization, the granular particles are subjected to an upward fluid flow which creates a drag force sufficient to support the weight of the particles [16]. Once the jet is halted, viscous and kinetic energy is lost, a general slope failure occurs and closures the fluidized bed. Consequently, the density of the fluidized area prior and after fluidization is expected to change.

Cone penetrometer test (CPT) characterization of the two sands used in these tests allowed density to be estimated prior and after fluidization. CPT results are presented in terms of the variation of tip cone resistance  $q_c$  with depth measured with a 8 mm diameter minicone ( $0.5 \text{ cm}^2$  cross section area) for tests carried out in fine and coarse, fluidized and non-fluidized sand (Fig. 9). In fine sand, the  $q_c$  values for both medium and dense samples increase linearly with depth. The relative density ( $D_r$ ) of the undisturbed denser sand is of about 90%, corresponding to  $q_c = 680 \text{ kPa}$  at the mid-height of sample in the centre of the tank, and reduces to  $q_c = 250 \text{ kPa}$  for a medium density of 50%. After fluidization the cone resistance reduces to an average value of about  $q_c = 125 \text{ kPa}$  for both samples (dense and medium initial densities), which corresponds to fluidized densities of about 30%.

Similar results have been obtained for coarse sand, as indicated by the measurements of cone resistance  $q_c$  for medium dense samples (Fig. 9b). The coarse sand produces profiles with many small sharp peaks and troughs due to the large size of grains in respect to the diameter of the cone. The initial measured relative density of 50%

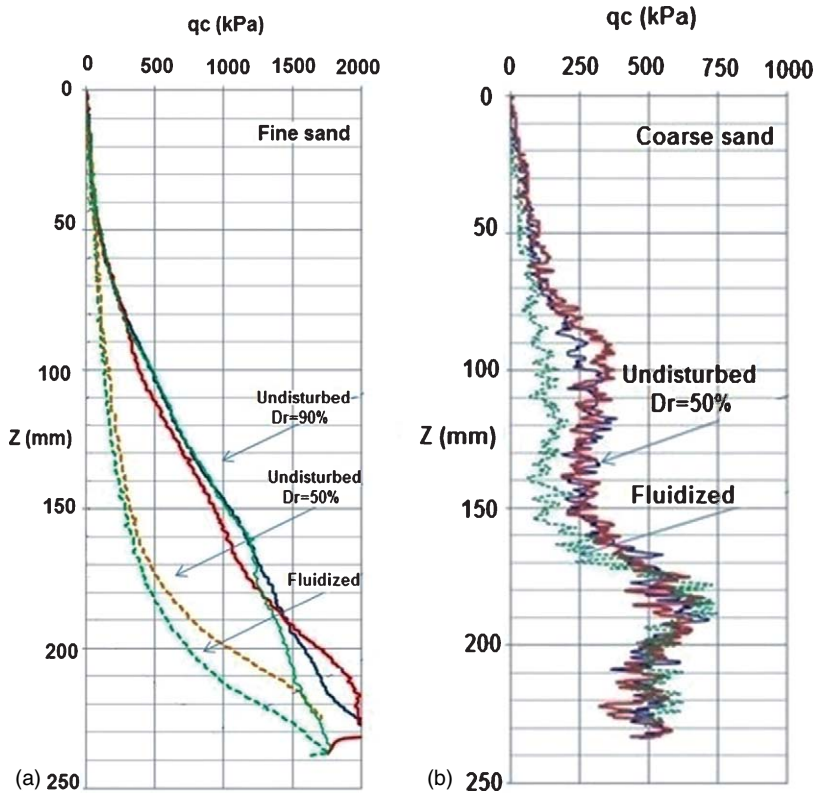


Fig. 9. CPT tests carried out in fluidized and non-fluidized (a) fine and (b) coarse sand.

corresponds to  $q_c$  of about 312.5 kPa and drops to approximately 150 kPa after fluidization. A depth of about 180 mm corresponds to the maximum jet penetration depth and, therefore, below this depth the fluidized and non-fluidized profiles coincide.

Boundary conditions would have to be considered when predicting relative density from penetration measurements in small tanks (e.g. [29]). Since the objective of the present study is simply to compare tests under different densities, the relative density ( $D_r$ ) of these tested sands is related to the CPT  $q_c$  values by equation 4:

$$D_r = \left( \frac{q_c}{\alpha \sigma_{vo}} \right)^{0.5} \quad (4)$$

Values of  $\alpha$  corresponding to 700 and 1300 have been calibrated for fine and coarse sand respectively. The  $\alpha$  value of coarse sand is greater than the corresponding value for fine sand due to higher grains to diameter ratio, as previously mentioned.

## 6. Implications to design

The shaft friction developed on displacement piles is related to the degree of soil displacement imparted during pile installation. Factors to be considered in the development of shaft friction prediction methods are radial effective stress at failure, interface friction angle between the soil and pile, type and number of cycles imposed during drivability, mode of loading, among others (e.g. [5, 19, 25, 26]). Because of the shortage of high quality measurements of shaft friction on tension jacked steel piles and the lack of consistent data on fluidization piles, the analysis of the potential implications of the fluidization process to foundation design is investigated in the present work by a series of tension load tests carried out in fine sands.

Table 3  
Load tests in fluidized and no-fluidized fine sand

N° tests	Test	Initial Dr (%)	$d_e$ (mm)	$Q_o$ (L/min)	L (mm)
35	No-fluidized	90	14.0–16.0	–	100–500
55	No-Fluidized	50	6.0–16.0	–	100–820
7	Fluidized	90	16.0	1.0	330–460
29	Fluidized	50	6.0–16.0	0.7–1.6	295–820

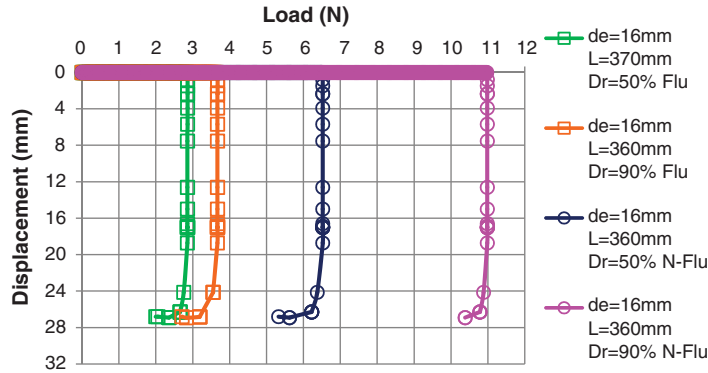


Fig. 10. Typical results of load-displacement curves.

The work comprises 90 tests in hydraulic displacement piles (jacked piles), immediately and 24 hours after pile driven, and 36 tests in fluidized piles, by suspended tubes and piles lowered into the ground by the own self-weight during fluidization, 24 hours after pile installation, both in the center position inside the tank. The testing programme described in Table 3 corresponds to tests performed in fine sand with initial sand density of 50% and 90%. Loads were applied in stages and increased up to failure, as illustrated by the typical results of load-displacement curves shown in Fig. 10. Being load control, tests provide reliable and accurate measurements of maximum loads but do not allow brittle post-peak behavior to be detected, particularly for piles in denser sand. The uplift displacement-to-diameter ratios at failure are of the order of 0.01% and at this stage the maximum load characterizes the pile shaft uplift capacity,  $Q_f$ .

A possible reason for foundations submitted to tensile loading presenting displacements that are smaller than those with the same compressive load is that shear strains under uplift loading are more pronounced than volumetric strains in contributing to displacements. In the case of fine sand, the combination of pile roughness (smooth pile) and the fine grain size produces a thin shear band at the soil-pile interface, thus yielding to very small displacements to reach failure conditions. Coarse sand, specially for dilative interface, would exhibit distinct pile response.

In this set of experiments it has been observed that, for each relative density, values of  $Q_f$  measured immediately and 24 hours after pile installation in non-fluidized soil remained unchanged, as expected, since the material has high permeability and fast dissipation of initial excess pore pressures. The impact of the fluidization process on overall shaft capacity is considerable, reflecting the changes in sand density ( $D_r$ ). In addition, given to the laws of similarity, values of  $Q_f$  are shown to be dependent on pile diameter ( $d_e$ ) and length ( $L$ ) and independent from flow rate ( $Q_o$ ), as demonstrated in Fig. 11 (a, b and c).

From limit equilibrium analysis, shaft capacity of the tested piles is expressed as:

$$Q_f = \pi D \int \tau_f dz \quad (5)$$

where

$$\tau_f = \sigma'_{rf} \tan \delta = K_s \sigma'_v \tan \delta \quad (6)$$

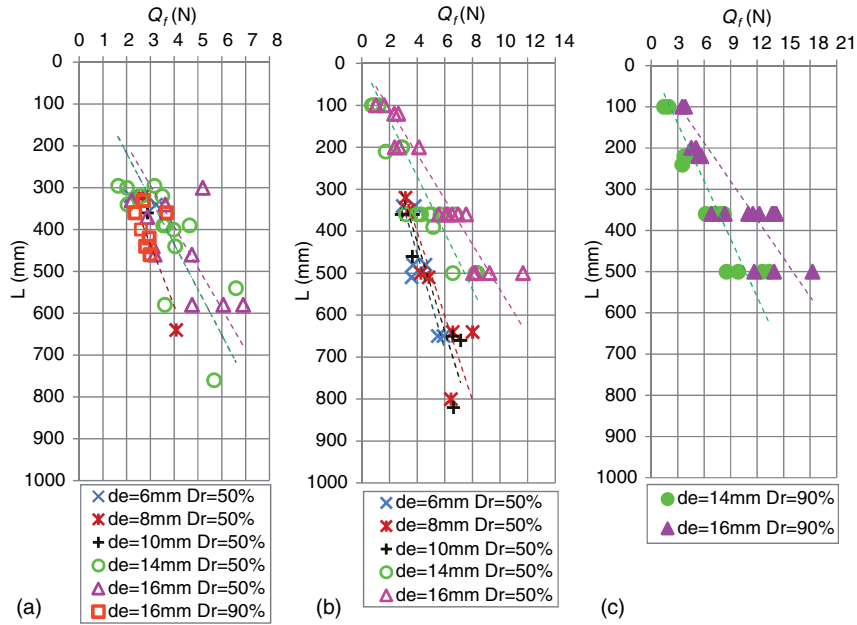


Fig. 11. Pile shaft uplift capacity ( $Q_f$ ) versus pile length inside sand specimen ( $L$ ) in (a) fluidized (b, c) non-fluidized fine sand.

being

- $\delta$  = interface friction angle between soil and pile shaft
- $\sigma'_{rf}$  = radial effective stress at failure
- $\sigma'_v$  = effective overburden stress
- $K_s$  = coefficient of lateral earth pressure (ratio of horizontal to vertical normal effective stress)

One simplifying assumption in the interpretation of these model pile tests is to assume  $\tau_f$  constant over the pile shaft for both fluidized and non-fluidized piles. The effective vertical stress corresponds to the overburden stress, despite the fact that in sand unit shaft resistance does not necessarily increase linearly with depth (e.g. [15, 31]).

For the fine sand, the interface friction angle  $\delta$  is assumed to be the same as the critical state friction angle ( $\phi_{cv} = 26.6^\circ$ ), as obtained from triaxial and ring shear tests conducted by Consoli et al. [7]. The assumption of  $\delta = \phi_{cv}$  is justified by the very large vertical shear strains developed near the pile shaft at ultimate load levels, expressed in terms of the constant-volume (or critical-state) friction angle (e.g. [17, 18]). It is supported by direct interface shear tests [14, 17] and in close agreement to recommendations from by the American Petroleum Institute code of practice [2].

Within these assumptions, the average coefficient of lateral earth pressure  $K_s$  for each test is calculated using equation 6 (Fig. 12a, b and c) for fluidized and non-fluidized fine sand.  $K_s$  values at full mobilisation of limit shaft resistance are shown to increase with increasing sand relative density and decrease with increasing initial effective overburden stress. At higher stresses (i.e. longer piles)  $K_s$  values become relatively constant, reaching minimum of 0.15, 0.30 and 0.50 for fluidized, non-fluidized  $Dr = 50\%$  and non-fluidized  $Dr = 90\%$  sand specimens, respectively. These measured values of  $K_s$  are slightly lower than early reported data and yield  $K_s/K_0$  ratios of the order of 1.0 and 2.0 for non-fluidized sand at 50% e 90% respectively (e.g. [28]). Maximum  $K_s$  values order of 1.5 in non-fluidized sand ( $K_s/K_0 \sim 4.5$ ) and have been obtained and very low confining stresses.

Although grain size effects become negligible for  $d_e/d_{50}$  larger than 100 to 200 [8, 10], these calculated values should be considered as preliminary indications of  $K_s$  and further validation in larger model scales is necessary before their use in engineering design.

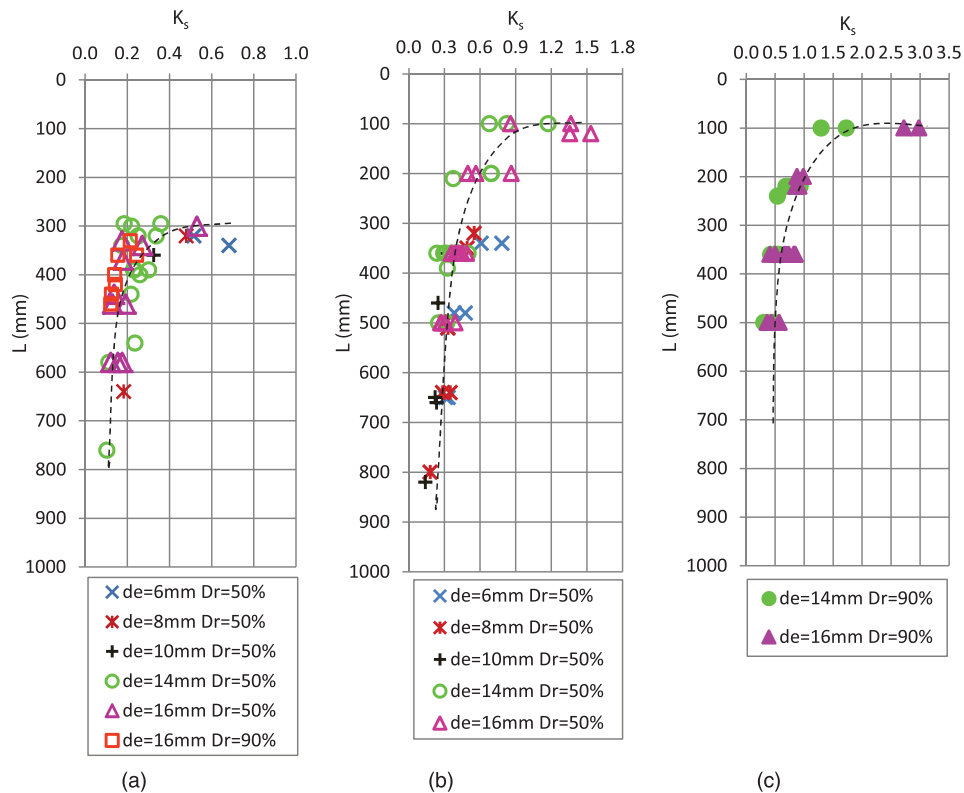


Fig. 12. Coefficient of lateral earth pressure ( $K_s$ ) versus pile length inside sand specimen ( $L$ ) in (a) fluidized (b, c) non-fluidized fine sand.

## 7. Conclusions

This paper reports results from small scale laboratory model tests carried out to investigate the mechanisms of pile installation in fluidized sands. Considering that the research aims at supporting the prediction the geometry and density of fluidized cavities for future use in foundation design, attention has been given to the analysis of the fluidization jet penetration depth and fluidization radii at the pile tip. These variables are shown to be controlled by combined effects of jet velocity and the ratio of particle and jet diameter, being conveniently expressed by the Froude number of particles. Once the prediction of fluidized zone geometry from system variables was completed, the additional requirement was referred to the density of the fluidized sand bed prior and after fluidization. Despite the initial density, the sand approaches the same low density after fluidization which is a state close to critical state soil conditions. Variation in density impacts the prediction of pile bearing capacity: the shaft tensile capacity of jacked piles is shown to reduce considerably when compared to the same pile installed in the ground by fluidization.

## Acknowledgments

The authors wish to express their gratitude to the Brazilian Oil Company Petrobras for the financial support of the research group (UFRGS Ref. 4600346071: Offshore Technology: Foundations, fluidization and ground improvement).

## References

- [1] Aderibigbe OO, Rajaratnam N. Erosion of loose beds by submerged circular impinging turbulent jets. *J of Hydraulic Research*. 1996;34(1):19-33.
- [2] API RP 2A. Recommended practice for planning, designing, and constructing fixed offshore platforms. 1991; 19th edition.

- [3] Bass DH, Hastings NA, Brown RA. Performance of air sparging systems: A review of case studies. *J of Hazardous Materials*. 2000;72:101-119.
- [4] Bienen B, Gaudin C, Cassidy MJ. The influence of pull-out load on the efficiency of jetting during spudcan extraction. *Applied Ocean Research*. 2009;31(3):202-211.
- [5] Broms BB. Lateral resistance of piles in cohesionless soils. *J Soil Mech Found Engng*. 1964;90(3):123-156.
- [6] Cline SR, Reed BE. Lead removal from soils via bench-scale soil washing techniques. *J Environmental Engineering*. 1995;121(10):700-705.
- [7] Consoli NC, Casagrande MDT, Coop MD. Performance of a fiber reinforcement sand at large shear strains. *Geotechnique*. 2007;57(9):751-756.
- [8] Foray P, Balachowski L, Rault G. Scale effect in shaftfriction due to the localization of deformations. *Centrifuge*. 1998;98:211-216. Rotterdam: Balkema.
- [9] Gabr MA, Bordenn RH, Smith AW, Denton RL. Laboratory Characterization of Jetting-Induced Disturbance Zones. *Soils Improvement Geo-Denver 2007*. Colorado, USA, 2007; 18-21.
- [10] Garnier J, Konig D. Scale effects in piles and nailsloading tests in sand. *Centrifuge 98* (Kimura, Kusakabe & Takemura, 1998;205-210. Rotterdam: Balkema.
- [11] Gaudin C, Bienen B, Cassidy J. *Géotechnique*. 2011;61(12):1043-1054.
- [12] Griffiths RA. Soil-washing technology and practice. *J Hazardous Materials*. 1995;40:175-189.
- [13] Hagyard T, Gilmour IA, Mottram WD. A proposal to remove sand bars by fluidization. *New Zealand Journal of Science*. 1969;12:851-864.
- [14] Jardine RJ, Chow FC. *New Design Methods for Offshore Piles*. Marine Technology Directorate Ltd., MTD 96/103, London, 1996.
- [15] Kerizel J. Foundation profondes en milieu sableux. *V Int Conf Soil Mech Found Engng*. 1961;2:73-83.
- [16] Leva M. *Fluidization*, McGraw-Hill Book Co., New York, 1959, 327p.
- [17] Lehane BM, Jardine RJ, Bond AJ, Frank R. Determination of shaft friction in sand from instrumented pile tests. *J Geotechnical Eng ASCE*. 1993;121(8):1449-1452.
- [18] Loukidis D, Salgado R. Analysis of the shaft resistance of non-displacement piles in sand. *Geotechnique*. 2008;58(4):283-296.
- [19] Meyerhof GG. Penetration tests and bearing capacity of cohesionless soils. *J Soil Mech Found Eng*. 1956;82(1):1-19.
- [20] Mezzomo SM. Study of fluidization using water jets in sand. MSc Thesis, Graduation Program in Civil Engineering, Federal University of Rio Grande do Sul, Brazil. In Portuguese, 2009.
- [21] Niven RK. *In situ* multiphase fluidisation (“upflow washing”) for the remediation of diesel and lead contaminated soils. PhD Thesis, University of New South Wales, Sydney, Austrália, 1998, pp. 548.
- [22] Niven RK, Khalili N. *In situ* fluidisation by a single internal vertical jet. *J of Hydraulic Research*. 1998;36(2):199-228.
- [23] O’Donoghue T, Trajkovic B, Piggins J. Sand bed response to submerged water jet. *Proceedings of the Eleventh Int Offshore & Polar Engineering Conf Stavanger*, 2001; pp. 66-72.
- [24] Otten A, Alphenaar A, Pijls C, Spuij F, de Wit H. *In Situ* Soil Remediation, Kluwer Academic Publishers, Boston, 1997.
- [25] Peck RB, Hansen WE, Thorburn TH. *Foundation Engineering*. New York, Wiley, 1974.
- [26] Poulos HG. *Pile Behaviour – Theory and Application*. *Geotechnique*. 1989;39(3):365-415.
- [27] Rajaratnam N. *Turbulent jets*. Elsevier Scientific Publishing Company, New York, 1976; 304pp.
- [28] Salgado R. *The Engineering of Foundations*. McGraw-Hill Science/Engineering/Math; 1 edition, 2006; 896 pp.
- [29] Schnaid F, Houlsby GT. An Assessment of Chamber Size Effects In The Calibration of *In Situ* Tests in Sand. *Geotechnique*. 1991;41(4):437-445.
- [30] Stracke F. Fluidization of sand associated to injection of cement agent for applying in offshore structures. MSc Thesis, Graduation Program in Civil Engineering, Federal University of Rio Grande do Sul, Brazil. In Portuguese, 2012.
- [31] Vésic AS. A study of bearing capacity of deep foundations. Proj B-189 Report, School of Civil Eng Georgia Inst Tech. USA, 1967.
- [32] Weisman RN, Collins AG, Parks JM. Maintaining tidal inlet channels by fluidization. *J of the Waterway, Port, Coastal and Ocean Division ASCE*. 1982;108(4):526-538.
- [33] Weisman RN, Lennon GP, Roberts EW. Experiment on fluidization in unbounded domains. *J of Hydraulic Engineering ASCE*. 1988;114(5):502-515.
- [34] Westrich B, Kobus H. Erosion of a uniform sand bed by continuous and pulsating jets. *Proceedings of Int Association of Hydraulic Research Cong*. 1973;1(13):1-3.